Journal of Materials Chemistry B

PAPER

View Article Online
View Journal | View Issue

Cite this: J. Mater. Chem. B, 2014, 2, 6652

Cross-linked self-assembled micelle based nanosensor for intracellular pH measurements†

E. K. Pramod Kumar,[ab] Rikke Vicki Søndergaard,[ab] Barbara Windschiegl,[a] Kristoffer Almdal[a] and Thomas L. Andresen*[ab]

Received 21st March 2014
Accepted 23rd July 2014

DOI: 10.1039/c4tb00446a

www.rsc.org/MaterialsB

A micelle based nanosensor was synthesized and investigated as a ratiometric pH sensor for use in measurements in living cells by fluorescent microscopy. The nanosensor synthesis was based on self-assembly of an amphiphilic triblock copolymer, which was chemically cross-linked after micelle formation. The copolymer, poly(ethylene glycol)-*b*-poly(2-aminoethyl methacrylate)-*b*-poly(styrene) (PEG-*b*-PAEMA-*b*-PS), was synthesized by isolated macroinitiator atom transfer radical polymerization that forms micelles spontaneously in water. The PAEMA shell of the micelle was hereafter cross-linked by an amidation reaction using 3,6,9-trioxaundecandioic acid cross-linker. The cross-linked micelle was functionalized with two pH sensitive fluorophores and one reference fluorophore, which resulted in a highly uniform ratiometric pH nanosensor with a diameter of 29 nm. The use of two sensor fluorophores provided a sensor with a very broad measurement range that seems to be influenced by the chemical design of the sensor. Cell experiments show that the sensor is capable of monitoring the pH distributions in HeLa cells.

Introduction

In cells, intracellular pH plays an important role for the structural stability and function of proteins, in organelles such as lysosomes and mitochondria, as well as in cell cycle progression and apoptosis.[1–4] In nanoparticle based drug delivery systems, the pH in endosomes and lysosomes has been a target for controlling drug release specifically in diseased cells, and an increased understanding of pH profiles in the endosome-lysosome pathway is important for future development of pH sensitive nanocarrier systems.[5] A number of fluorescent probe based nanosensors have been developed in the last decade for intracellular pH measurement by various groups and the efforts in this area is high as several challenges remains in creating highly reproducible sensor particles that interact with cells in a controlled way.[6–11] A long term objective is furthermore to develop nanosensors that can be used for *in vivo* measurements,[12] where polymeric micelles with a PEG corona may be of particular interest due to their low immunogenicity and ability to overcome clearance by macrophages.[13,14] In addition, difficulties in synthesizing well defined nanosensors have enhanced the interest in developing self-assembled polymeric micelles with high structural control.[15,16] However, such micelles can be prone to disintegration under diluted biological conditions, which hampers their use as nanosensors and more advanced strategies are therefore needed.

Controlled radical polymerization, especially redox-active transition metal complex catalyzed atom transfer radical polymerization (ATRP)[17] can provide well defined block co-polymers for use in advanced functional materials with high control of composition and molecular architecture. Amphiphilic block copolymers having definite hydrophilic to hydrophobic block size ratios can provide a variety of structural morphologies on nanoscale such as micelles, lamellae, tubes and rods.[18,19] In a biological setting these structures behave differently and it is an interesting perspective to develop nanosensors based on different morphologies using self-assembly principles. In addition, self-assembly of nanostructures can enhance the control of the surface chemistry in comparison to other methods[20] and thereby provide a platform for introducing biological targeting molecules. However, the self-assembly also introduces a risk of disintegration and post-cross-linking of nanoparticle constructs that are designed for self-assembly is therefore highly important to ensure nanosensor integrity.[21,22] The focus of this article is to design a nanosensor that is synthesized by the use of triblock copolymers that self-assemble into core–shell–corona micelles in water. In the shell region we installed functional groups that allowed for chemical cross-linking of the micelle to ensure nanosensor integrity under biological conditions. The formed cross-linked micelle could further be post-functionalized with fluorescent dyes that are

[a]DTU Nanotech, Department of Micro-and Nanotechnology, Technical University of Denmark, Building 423, 2800 Lyngby, Denmark. E-mail: thomas.andresen@nanotech.dtu.dk

[b]Center for Nanomedicine and Theranostics, Technical University of Denmark, Building 423, 2800 Lyngby, Denmark

† Electronic supplementary information (ESI) available: See DOI: 10.1039/c4tb00446a

sensitive to pH resulting in a nanosensor with a broad pH spectrum that allowed for cellular measurements.

Experimental section

Materials

Styrene (99.5%) was obtained from Fluka and the radical inhibitors were removed by passing through a column filled with basic alumina. 2-Aminoethyl methacrylate hydrochloride (AEMA·HCl) (90%), bis(*tert*-butyl) dicarbonate (99%), triethylamine (TEA) (99.5%), 2-bromo-isobutyryl-bromide (98%), CuCl (99.995%), 2,2′bipyridyl (bpy) (99%), PMDETA (99%), $CuCl_2$ (99.995%), trifluoroacetic acid (TFA) (99%), dialysis tubing (MWCO = 12 kDa), *N*-(3-dimetylaminopropyl)-*N*′-ethyl-carbodiimide methiodide (EDC·MeI), rhodamine B isothiocyanate (RhBITC) and fluorescein 5(6)-isothiocyanate (FITC) (90%) were purchased from Sigma Aldrich and used as obtained. 3,6,9-Trioxaundecandioic acid (TUDA) was purchased from iris biotech GMBH, Oregon Green 488 isothiocyanate (OGITC) was purchased from Invitrogen, and CH_3O-PEG-OH (poly (ethylene glycol) monomethylether (M_n = 5000, was measured to M_n = 5500 by NMR) was from Fluka. Solvents used for atom transfer polymerization (ATRP) were purified by distillation over the drying agents indicated in parentheses MeOH ($Mg(OMe)_2$), DMF (CaH_2). Solvents are stored over molecular sieves (MeOH 3 Å and DMF 4 Å) and transferred under argon. Other solvents and commercially available chemicals were used as obtained. Water used was collected from Millipore and aqueous buffer solutions were prepared from the reported procedures.

Instrumentation details

^{1}H-NMR spectra were recorded on a Bruker 250 MHz in solvents as indicated. The chemical shifts (δ) were given in ppm relative to TMS. The residual solvent signals were used as a reference, and the chemical shifts converted into TMS scale ($CDCl_3$: δ_H = 7.24 ppm, ^{6}d-DMSO: δ_H = 2.50 ppm, D_2O: δ_H = 4.79 ppm). Infrared spectra were recorded using a Perkin Elmer FT-IR Spectrometer (KBr pellets method) and the wavenumbers of recorded IR signals quoted in cm^{-1}. The number-average molecular weight (M_n), weight average molecular weight (M_w), and polydispersity (M_w/M_n) of block copolymers were determined by GPC analysis based on poly styrene calibration standards. Measurements were carried out by using a Mixed-D GPC column from Polymer Laboratories (7.4 × 300 mm) and a RID10A-SHIMADZU refractive index detector. DMF with 50 mM LiCl solution was used as eluent (1 mL min^{-1}) at 25 °C. LiCl was used to minimize polymer aggregation in DMF and hence misleading micelle formation (hydrodynamic diameter issues) can be avoided. Hydrodynamic diameters (D_h) and size distributions of the amphiphilic colloidal dispersion in MilliQ water at 25 °C were determined by Brookhaven ZETA PALS instrument. Calculation of the particle size distribution and distribution averages were performed with the ISDA software package (from Brookhaven) through CONTIN particle size distribution analysis routines. All determinations were made in triplicate for duration of 2 minutes each. Zeta potential measurements were carried out using a Brookhaven ZETA PALS analyzer. The measurements were made in MilliQ water at 25 °C and the zeta potential (ξ) was calculated using the Smoluchowski equation, *i.e.*, electrophoretic mobility (μ) = $\xi\varepsilon/\eta$, where η and ε are the absolute viscosity and dielectric constant of the medium, respectively. The mean value of ξ was calculated from ten data accumulations. Fluorescence measurements were carried out using an EDINBURGH F-900 fluorometer. A PSIA XE-150 microscope was used for AFM measurements. Argon atmosphere (99.9999%) used in the reactions was provided by AGA Denmark.

Synthesis of PEG_{127}-*b*-$PAEMA_{12}$-*b*-PS_{28}

The macroinitiator $PEG_{127}Br$ and the monomer 2-[*N*-(*tert*-butoxycarbonyl)amino]ethyl methacrylate (AEMA(Boc)) were synthesized by previously reported procedures.[23,24]

PEG_{127}-*b*-P(AEMA(Boc))$_{12}$Cl. PEG_{127}-Br (2 gram, 0.36 mmol), AEMABoc (852 mg, 5 mmol), 2,2′bipyridyl (122 mg, 0.76 mmol) and 10 mL dry MeOH were added to a 25 mL schlenk flask equipped with a stir bar. The flask was frozen in liquid nitrogen and CuCl catalyst (40 mg, 0.40 mmol) was added. The reaction mixture was degassed with 3 freeze–pump–thaw cycles (each 15 minute long) to remove the oxygen and the polymerization was carried out at 40 °C for 24 h under argon atmosphere. The dark brown reaction solution was passed through a silica gel column to remove the copper catalyst using MeOH as solvent. On exposure to air, the solution turned to blue, which indicated the aerial oxidation of the Cu(I) catalyst. After the removal of most of the MeOH by rotary evaporation, the polymer was precipitated into excess cold diethyl ether. The precipitate was then isolated by filtration and dried under vacuum to yield 1.86 g (62%) of the diblock copolymer. ^{1}H-NMR (250 MHz, $CDCl_3$): δ = 5.50 (br s, –N*H*), 4.0 (br s, –O$CH_2$$CH_2$NH), 3.63 (s, –$CH_2$$CH_2$O), 3.37 (br m, –OCH$_2$$CH_2$NH, –O$CH_3$), 1.82 (br, –$CH_2$ backbone), 1.43 (s, –C(CH_3)$_3$), 1.11–0.81 (m, –C(CH_3)$_2$, –CH_3 backbone); FT-IR (cm^{-1}): 3387, 2892, 1716, 1520, 1466, 1391, 1361, 1342, 1279, 1241, 1150, 1112, 1060, 996, 965, 843; M_n (NMR) = 8340; M_n (GPC) = 5600, M_w = 6460, PD (M_w/M_n) = 1.15.

Synthesis of PEG_{127}-*b*-P(AEMA(Boc))$_{12}$-*b*-PS_{28} (1). PEG_{127}-*b*-P(AEMA(Boc))$_{12}$-Cl (1.0 g, 0.12 mmol), styrene (0.48 mL, 4.2 mmol), $CuCl_2$ (13 mg, 0.096 mmol), PMDETA (0.087 mL, 0.42 mmol), and 3 mL of DMF were added into a 25 mL schlenk flask equipped with a stir bar. The flask was frozen in liquid nitrogen and the CuCl catalyst (12 mg, 0.12 mmol) was added to it. After being degassed with 3 freeze–pump–thaw cycles (each cycle was 15 minutes long) to remove the oxygen, the polymerization was carried out at 130 °C for 27 h under an argon atmosphere. The reaction mixture was concentrated under vacuum and the polymer was precipitated in cold diethyl ether. The precipitate was dried under vacuum to yield 0.74 g (55%) of the triblock copolymer. ^{1}H-NMR (250 MHz, ^{6}d-DMSO): δ = 7.3–6.3 (m, ArH), 3.84 (br, –OCH$_2$CH$_2$NH), 3.50 (s, –CH$_2$CH$_2$O), 3.18 (br, –OCH$_2$-CH$_2$NH), 2.10–1.60 (br, CH_2 and –CH backbone), 1.36 (s, –C(CH_3)$_3$), 1.20–0.59 (m, –CH_3 backbone); FT-IR (cm^{-1}): 3370, 3025, 2887, 1716, 1602, 1496, 1451, 1342, 1279, 1243, 1146,

1105, 961, 841; M_n (NMR) = 11 250; M_n (GPC) = 9280, M_w = 11 800, PD (M_w/M_n) = 1.27.

PEG_{127}-*b*-$PAEMA_{12}$-*b*-PS_{28} (2). The triblock copolymer, PEG-*b*-PAEMA(Boc)-*b*-PS (1.0 g, 0.088 mmol) was dissolved in 4 mL of DCM, followed by 4 mL TFA added drop wise, and the mixture was stirred at room temperature for 10 h. After evaporating most of the solvent under reduced pressure, the polymer was precipitated into excess cold diethyl ether and dried under vacuum. The complete de-protection of the amino group was confirmed by the disappearance of the Boc group signal at δ 1.36 (s, $-C(CH_3)_3$) ^{1}H-NMR (250 MHz in ^{6}d-DMSO) and qualitatively by conducting a Kaiser test.[25] ^{1}H-NMR (250 MHz, ^{6}d-DMSO): δ = 7.3–6.3 (m, Ar*H*), 3.73 (br, $-OCH_2CH_2NH$), 3.50 (s, $-CH_2CH_2O$), 3.07 (br, $-OCH_2CH_2NH$), 2.10–1.60 (br, CH_2 and –C*H* backbone), 1.57–1.25 (br, $-NH_2$), 1.20–0.59 (m, $-CH_3$ backbone); FT-IR (cm^{-1}): 3439, 3021, 2910, 1733, 1692, 1602, 1494, 1453, 1350, 1277, 1245, 1150, 1109, 953, 843. A GPC chromatogram of the polymer is given in ESI Fig. S8† and compared to starting materials and synthesis intermediates.

Shell cross-linked micelle nanosensor (SCMN) 5 synthesis

The deprotected amphiphilic triblock copolymer PEG_{127}-*b*-$PAEMA_{12}$-*b*-PS_{28} (**2**) (100 mg, 0.0088 mmol) was dissolved in 10 mL DMF by stirring overnight. To the polymeric solution under stirring, 2 mL of MilliQ water was added dropwise within 30 minutes followed by 20 mL more MilliQ water added dropwise. The cloudy micelle solution was transferred into a dialysis tube of molecular weight cut off (MWCO = 12 kDa) and dialyzed against MilliQ water for 5 days. Number-averaged hydrodynamic diameters (D_h) and zeta potentials (ξ) were found to be 29 $\pm$ 2 nm and +29 $\pm$ 1 mV, respectively. The final block copolymer concentration after dialysis was 2 mg mL^{-1}. To the micelle solution (25 mL (50 mg, 0.0044 mmol, 0.053 mmol of amine)), 3,6,9-trioxaundecandioic acid (3.6 mg, 0.016 mmol) and 1-[3-(dimethylamino)propyl]-3-ethylcarbodiimide methiodide (9.5 mg, 0.032 mmol) was added and stirred at room temperature for 10 h. The reaction mixture was then dialyzed against MilliQ water for 3 days (D_h (number-averaged) = 24 $\pm$ 1 nm and ξ = +18 $\pm$ 2), then against 0.1 M carbonate buffer (pH = 9.6) for another 3 days. To 3 mL of the basic amphiphilic colloidal dispersion, RhBITC (0.014 mg, 0.0264 μmol), FITC (0.026 mg, 0.066 μmol) and OGITC (0.028 mg, 0.066 μmol) were added and stirred in the absence of light at room temperature for 12 h. The reaction mixture was transferred into a dialysis tube (MWCO = 12 kDa) and dialysis was conducted against 0.1 M carbonate buffer for 3 days, then against MilliQ water for another 5 days (D_h (Number-averaged) = 25 $\pm$ 2 nm and ξ = 16 $\pm$ 2 mV). The final nanosensor concentration was 1.9 mg of polymers per mL of water.

pH calibration curve from spectrofluorometer

The pH calibration curve was constructed by fluorescence measurements. 50 μl of the SCMN were added to 1 mL of buffer solutions having different pH. The nanosensor solutions were excited at 488 and 543 nm, successively. Fluorescence emission spectra of the nanosensors at different pH were plotted. From the fluorescence emission spectra of Fluorescein (FA), Oregon Green (OG) and Rhodamine (RhB), fluorescence intensity (I) ratios (I_{OG} + I_{FA})/I_{RhB} were calculated. These fluorescence intensity ratios were then plotted against corresponding pH to obtain the ratiometric pH calibration curves. The triple labelled nanosensor's calibration curve was fitted by the following equation,[11]

$$R = \frac{R_1}{10^{pK_{a1}-pH}+1} + \frac{R_2}{10^{pK_{a2}-pH}+1} + R_0$$

where, R is the ratio of emission intensities of the nanosensor excited at 488 (OG and FA) and 543 nm (RhB). pK_{a1} and pK_{a2} describes the specific pK_a values of the two pH-sensitive fluorophores (OG and FA) conjugated to the micelle. $R_{min} = R_0$ is the ratio for the fully protonated sensor flurophors and $R_{max} = R_0 + R_1 + R_2$ are the ratio for the fully deprotonated sensor fluorophores. More details are given in the ESI† (see calibration curve fitting).

Intracellular pH measurements

HeLa cells were maintained in DMEM supplemented with 10% fetal bovine serum and 100 UI mL^{-1} penicillin and streptomycin. Cell cultures were incubated in a 5% CO_2 humidified incubator at 37 °C. Cells were seeded on 9 mm cover glasses in 24 well plates at a density of 2×10^4 HeLa cells per well the day before treatment. Cells were incubated in the presence of 10 μg mL^{-1} nanoparticle for 20 hours at 37 °C. Cells were then washed three times with ice-cold phosphate buffered saline (PBS) supplemented with heparin (20 units per mL), once with PBS and kept in growth medium without phenol red and bicarbonate but supplemented with 30 mM HEPES for control of pH without CO_2 incubation for observation by confocal microscopy. Cells were either imaged immediately or treated with 100 nM Bafilomycin A_1 for 45 min. before imaging. The images were captured by a Leica TCS SP5 confocal microscope with a 63× water-immersion objective (Leica Microsystems, Germany). A calibration turve was obtained on the same day of the measurements by diluting the nanosensor in buffers (20 mM phosphate/20 mM borate/20 mM acetate/100 mM NaCl) with different pH to a final nanosensor concentration of 1.25 mg mL^{-1}. Images of nanosensor in buffer were acquired at the microscope with the same settings as for the cell measurements. Image analysis was performed as described previously[11] with a pixel based method resulting in images with pixels colored according to a pH scale and frequency histograms of pH for the different treatments.

Results and discussion

Synthesis and characterization of the shell cross-linked micelle nanosensor (SCMN)

Fig. 1 illustrates the design strategy of the ratiometric nanosensor that has been developed. The sensor design is based on a hydrophobic styrene core, a functionalizable shell layer and a PEG corona. The amphiphilic triblock copolymer, poly(ethylene glycol)$_{127}$-*b*-poly(2-[*N*-(*tert*-butoxycarbonyl)-amino]ethyl methacrylate)$_{12}$-*b*-poly(styrene)$_{28}$ (PEG_{127}-*b*-$PAEMA(Boc)_{12}$-*b*-PS_{28}) (**1**) was synthesized by isolated

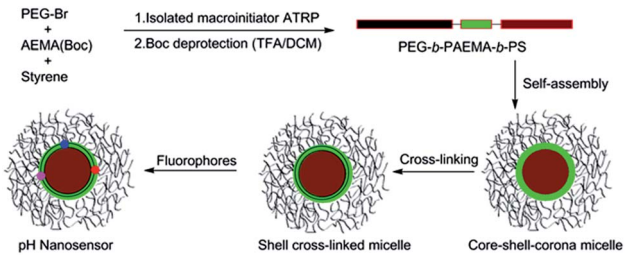

Fig. 1 Schematic representation of shell cross-linked core–shell–corona micelle pH nanosensor synthesis. AEMA(Boc) = 2-[*N*-(*tert*-butoxycarbonyl)amino]ethyl methacrylate.

macroinitiator atom transfer radical polymerization (Scheme 1) and the triblock copolymer was characterized by NMR and FT-IR spectroscopy. From the ^{1}H-NMR data (ESI Fig. S1†), the number-average degree of polymerization (DP_n) was determined. GPC analysis was used to calculate the polydispersity index (M_w/M_n) of the amphiphilic triblock copolymer. The NMR and GPC results are summarized in Table 1. The Boc groups from PEG-*b*-PAEMA(Boc)-*b*-PS were deprotected by TFA in DCM and the complete deprotection was confirmed by the disappearance of the Boc group signal at δ 1.36 ppm (s, $-C(CH_3)_3$) ^{1}H-NMR (250 MHz in ^{6}d DMSO) (ESI Fig. S2†).

The stepwise synthesis of the SCMN is shown in Scheme 2. First, the entropy driven self-assembly of PEG_{127}-*b*-$PAEMA_{12}$-*b*-PS_{28} (**2**) in water was achieved by dissolving the triblock copolymer in DMF that was slowly displaced by addition of excess water. The resulting polymeric micelle solution was then dialyzed against MilliQ water to remove the DMF. Stabilization of the resulting PEG_{127}-*b*-$PAEMA_{12}$-*b*-PS_{28} micelle (**3**) was achieved by covalent cross-linking between the unimers *via* cross-linking the shell region using an amidation reaction where water soluble 3,6,9-trioxaundecandioic acid was used as a cross-linking agent. The diacid cross-linker was first converted into *o*-acylisourea by treatment with 1-[3-(dimethylamino)propyl]-3-ethylcarbodiimide methiodide (EDC·MeI). This active ester

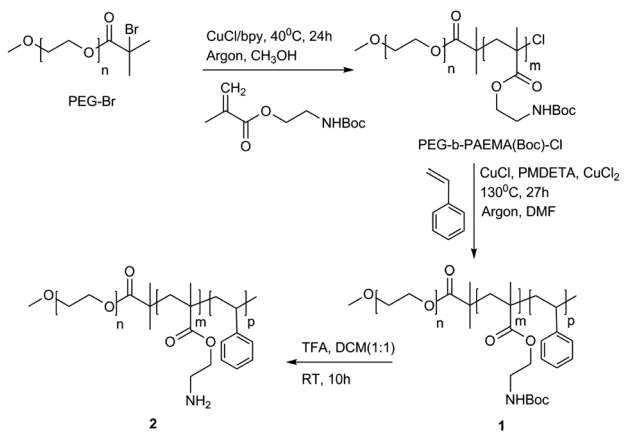

Scheme 1 Synthesis of PEG_{127}-*b*-$PAEMA_{12}$(Boc)-*b*-PS_{28} (**1**) by ATRP and PEG_{127}-*b*-$PAEMA_{12}$-*b*-PS_{28} (**2**) by deprotection of **1**. bpy = 2,2′-bipyridyl, PMDETA = *N*,*N*,*N*′,*N*″,*N*′-pentamethyldiethylenetriamine.

Table 1 Molecular weights of amphiphilic triblock copolymer, PEG_{127}-*b*-$PAEMA_{12}$(Boc)-*b*-PS_{28} (**1**)

M_n [a]	M_w [a]	M_w/M_n [a]	M_n [b]	n [c]	m [c]	p [c]
9280	11 800	1.27	11 250	127	12	28

[a] Determined by GPC. [b] Determined by NMR. [c] Number of repeating units of PEG block (n), PAEMA(Boc) block (m) and PS block (p).

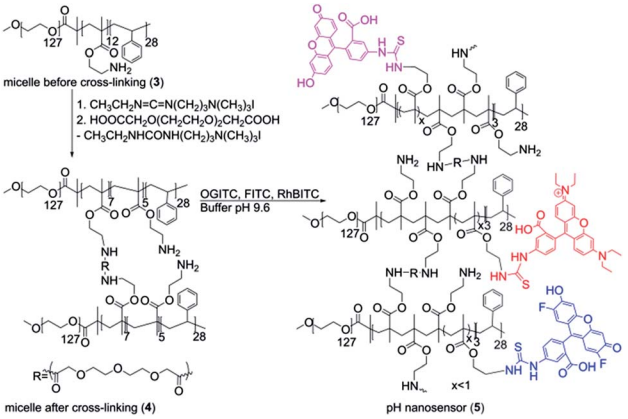

Scheme 2 Synthesis of shell cross-linked ratiometric micelle nanosensor. OGITC = Oregon Green isothiocyanate, FITC = Fluorescein isothiocyanate, and RhBITC = Rhodamine B isothiocyanate.

was then reacted with the free amino groups present at the shell layer (PAEMA shell) of the polymer micelle. Stoichiometrically, 60% of the amino groups were used for the cross-linking reactions. The shell cross-linked micelles were first dialyzed against MilliQ water to remove the urea by-products and then against 0.1 M carbonate buffer of pH 9.6. The cross-linked micelle **4** in basic buffer was converted into ratiometric pH nanosensor **5** by treatment with suitable ratios of pH sensitive Fluorescein isothiocyanate (FITC), Oregon Green isothiocyanate (OGITC), and pH insensitive reference fluorophore, Rhodamine B isothiocyanate (RhBITC). Some of the free amino groups present at the shell layer of the cross-linked micelle were used for nucleophilic attack of the central electrophilic carbon atoms of the pH sensitive and reference isothiocyanates. Excess un-reacted free dyes were removed by dialysis against carbonate buffer (0.1 M carbonate buffer (pH = 9.6)) followed by dialysis against MilliQ water, which gave a pH nanosensor dispersion in MilliQ water.

The morphology and size distribution of the micelle nanosensor was investigated by atomic force microscopy (AFM) under ambient conditions (Fig. 2). AFM images of the air dried nanosensor shows that the particles are round and relatively uniform in size. The spherical morphology can be observed in the phase contrast AFM image (Fig. 2b), which depicts the phase shift of the cantilever oscillation and visualizes differences in material properties of the sample. The AFM image also indicates low/no intermicellar cross-linking or aggregation of the nanosensor.

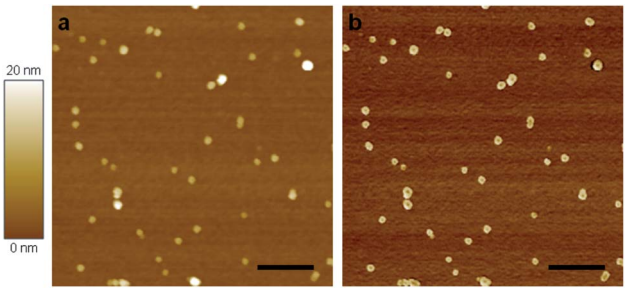

Fig. 2 Representative AFM images of shell cross-linked micelle nanosensor. (a) Topographic image and (b) phase contrast image. Scale bar 1 μm.

Characterizations of the shell cross-linked core–shell–corona micelles by ^{1}H-NMR was not possible; in D_2O the hydrophobic styrene core of the lyophilized micelle was not detectable, and NMR spectrum of the particles in ^{6}d-DMSO was inconclusive (ESI Fig. S3†). A FT-IR spectra of the lyophilized micelle after cross-linking showed additional overlapping amide I and II bands appearing at approximately 1640–1550 cm^{-1}. This confirmed the amide bond formation at the shell region of the micelle (ESI Fig. S4†).

The inner shell stabilization was not expected to considerably affect the outer corona mobility. Since the inner shell does not entropically impair the stabilizing capability of the hydrophilic PEG domains, an exclusive intramicellar cross-linking was anticipated. The intramicellar cross-linking was supported by dynamic light scattering (DLS) and zeta potential (ξ) measurements. DLS and ξ-potential measurements showed a small decrease in hydrodynamic diameter (D_h) and a substantial decrease in ξ-potential after shell cross-linking (Table 2). The decrease in charge density also confirmed the participation of amino groups of the shell domain in amidation cross-linking. Due to the low concentration of fluorophores in the nanosensor, the binding of fluorophores to the cross-linked micelle did not show any significant change in hydrodynamic diameter and ξ-potential.

DLS and size exclusion chromatography (SEC) further confirms the micelle cross-linking (Fig. 3). DLS measurements shows that cross-linked micelle **4** has a slightly lower particle size distribution than non-cross-linked micelle **3** (Fig. 3a), which indicates the absence of intermicellar crosslinking or aggregation after cross-linking. Furthermore, lyophilized cross-linked and non-cross-linked micelles had different solubility in THF. The non-cross-linked micelle **3** was readily soluble in THF, whereas the cross-linked micelle **4** was sparingly soluble only by ultrasonication for 1 h at 60 °C. SEC studies of these solutions showed different elution time for cross-linked and non-cross-linked micelles (Fig. 3b), which indicates a higher molecular weight for cross-linked micelle due to successful cross-linking between the unimers. Micelle cross-linking was also confirmed

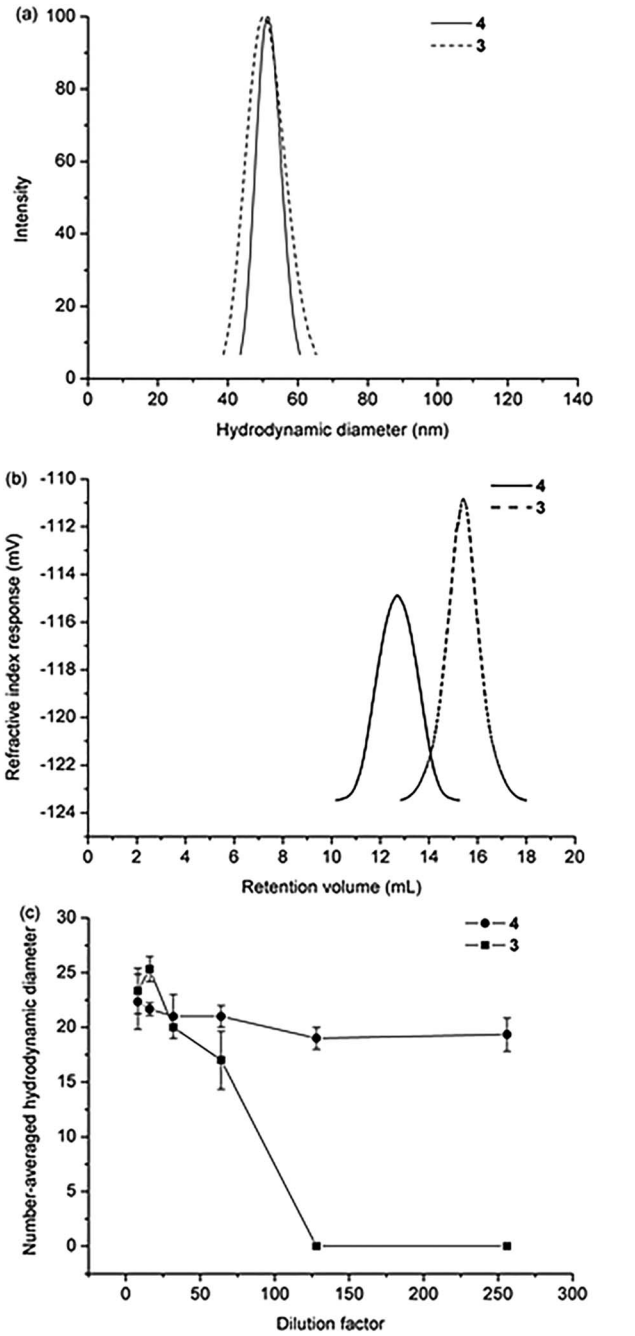

Fig. 3 (a) Particle size distribution by DLS in MilliQ water at 25 °C, (b) size exclusion chromatogram using DMF with 50 mM LiCl solution as eluent (0.5 mL min^{-1}) at 25 °C and (c) variation of number-averaged hydrodynamic diameter with respect to dilution/concentration of the non-cross-linked micelle **3** and cross-linked micelle **4**, respectively.

Table 2 DLS and Zeta potential measurements of nanoparticles at 25 °C in MilliQ water

Particles	DLS (D_h)[a] (nm)	Zeta (ξ)[b] (mV)
Micelle before cross-linking (**3**)	50 ± 2	29 ± 1
Micelle after cross-linking (**4**)	45 ± 1	18 ± 2
pH nanosensor (**5**)	46 ± 2	16 ± 2

[a] Intensity-averaged hydrodynamic diameters of nanoparticles by dynamic light scattering. [b] Zeta potential average from 10 measurements, each having 10 cycles.

by DLS measurement by investigating the variations of number-averaged hydrodynamic diameters of the micelle **3** and **4** as a function of dilution in MilliQ water (Fig. 3c). The micelle **3** and **4** were diluted with water from a concentration of 0.125 mg mL^{-1} to a concentration of 0.0039 mg mL^{-1} and number-averaged hydrodynamic diameters were measured. The measurement showed that the measurements of cross-linked micelle **4** were independent of dilution whereas the non-cross-linked micelle **3** was concentration dependent. The disintegration of non-cross-linked micelle into unimers occurred at a critical micelle concentration (cmc) of approximately 0.010 mg mL^{-1}.

For sensor synthesis, two pH sensitive dyes and one reference dye was chosen to expand the measurement range of the sensor and cover the full pH range inside cells. The choice of the pH sensitive dyes, oregon green and fluorescein, was based on their respective pK_a values of 4.7 and 6.4. These two dyes are thereby well suited to cover a pH range from approximately pH 4–7.5 when combined. As a pH insensitive reference dye we used rhodamine B. The usability of these dyes were tested before sensor synthesis by a fluorometer study where a calibration curve was formed by mixing the dyes in buffers of different pH. This study showed that the dyes can cover a pH range of approximately pH 4.1–7.7 (ESI Fig. S5†) when free in solution and excited at (λ_{ex}) 488 nm and 543 nm.

Conjugation of the pH sensitive dyes and reference dye to the shell region of the cross-linked micelle gave the nanosensor. A calibration curve was formed by adding the nanosensor to buffer solutions of different pH. The sensor was excited at (λ_{ex}) 488 nm and 543 nm on a fluorometer and emission scans were recorded. From the fluorescence emission spectra of the nanosensor (Fig. 4a) fluorescence intensity maxima (I) of pH sensitive fluorophores (I_{OG} + I_{FA}) and reference fluorophore (I_{RhB}) were determined. I_{OG} + I_{FA} represents the maximum emission intensity of the nanosensor when excited at 488 nm and I_{RhB} represents the maximum emission intensity of the nanosensor excited at 543 nm. Fluorescence intensity ratios (I_{OG} + I_{FA})/I_{RhB} were plotted against pH to obtain a pH calibration curve (Fig. 4b). The fitted calibration data shows that the sensor is sensitive in an interval between pH 3.5 and 7.5 with dual pK_a values (pK_{a1} = 4.3, pK_{a2} = 6.6, which are obtained as fitting parameters). This indicates that the fluorophore pK_a values can change due to the local chemical environment in the sensor as previously described,[8] which can expand the sensitivity range compared to using free dyes. In the present case the local chemical environment where the fluorophores are conjugated resulted in a change in the pK_a values of the fluorophores and a broadening of the nanosensor sensitivity range. The nanosensor can thereby cover a pH range from 3.5–7.5.

For comparison we also synthesized a sensor with only fluorescein and rhodamine B conjugated in the shell region of the micelle. As expected this sensor covered a much smaller pH interval from approximately 5.8 to 7.8 (ESI Fig. S6†).

The response time and reversibility of the pH nanosensor was also tested by fluorescence measurements (Fig. 5a and b). This shows the nanosensors respond quickly (in less than a second) towards a change in pH and are reversible between two pH's within the pH range.

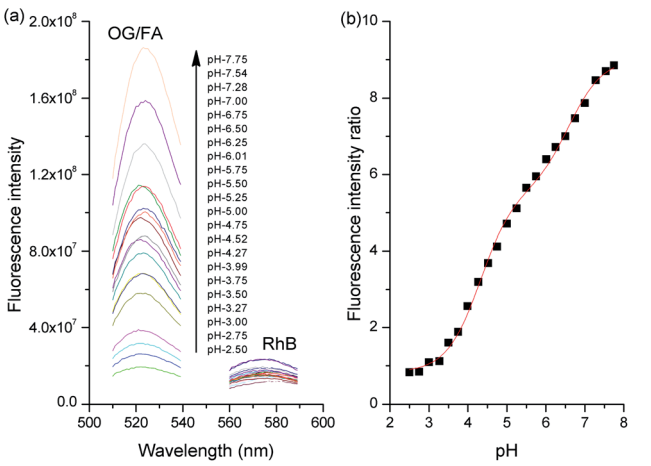

Fig. 4 (a) Fluorescence emission curve for the pH nanosensor. (b) pH calibration curve of the nanosensor made by plotting fluorescence intensity ratio (IOG + IFA/IRhB) against pH. OG = Oregon Green, FA = Fluorescein, RhB = Rhodamine B. The calibration data was used to find the best fit sigmoid curve using the formula, $R = R1/(10\text{^}(pK_{a1}\text{-pH}) + 1) + R2/(10\text{^}(pK_{a2}\text{-pH}) + 1) + R0$.

Intracellular pH measurements

The sensor is spontaneously taken up by the HeLa cells into small compartments probably through endocytosis due to the cationic surface chemistry of the sensor. After 20 hours, punctuate structures in the cytosol mainly around the nucleus are labelled. Fig. 6a show representative pH images of two cells, one without treatment (−Baf) and one after treatment with bafilomycin A_1 (+Baf). Cells were imaged by sequential scanning of the green pH sensitive fluorophores and the red reference fluorophore. The intensity ratio of green to red for each pixel was converted to pH *via* the calibration curve (ESI Fig. S7†) and the single pixels were thus colored according to a linear pH scale. The low pH of approx. 4.3 in the untreated cells and the punctuate pattern indicates that the sensor resides in the lysosomes.

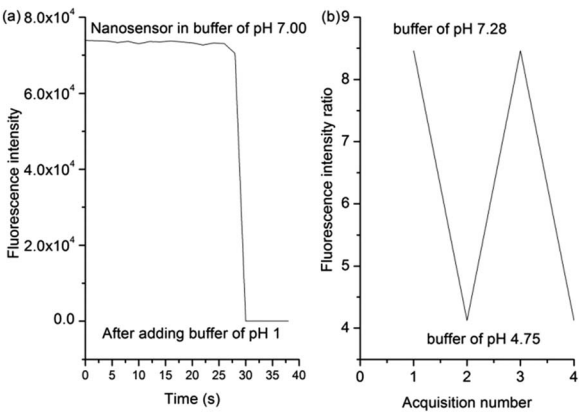

Fig. 5 (a) Response time of the nanosensor towards changes in pH. (b) Reversibility of the nanosensor, tested by repeatedly measuring the fluorescence intensity ratio (I_{OG} + I_{FA}/I_{RhB}) between two different pH's.

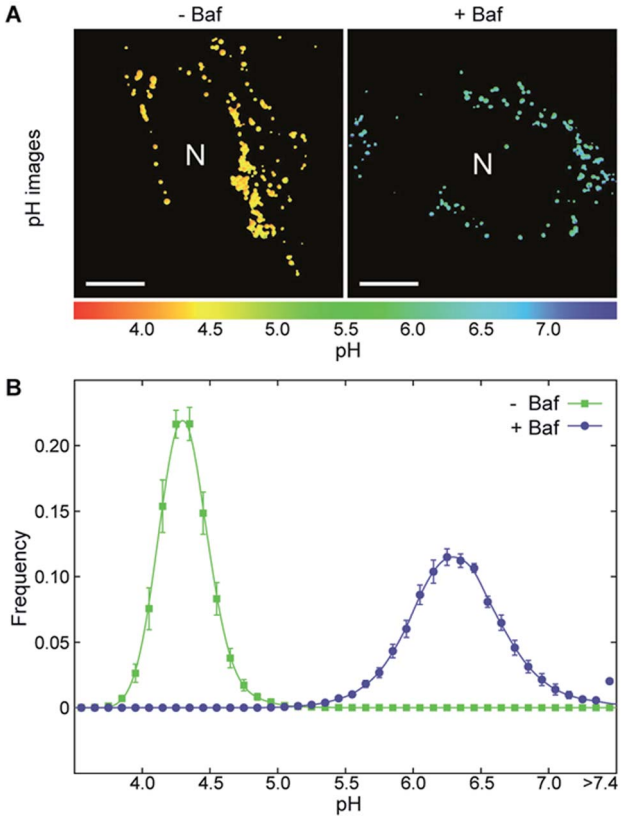

Fig. 6 HeLa cells were treated with nanosensor for 20 h, then washed and either imaged immediately or treated with 100 nM Bafilomycin A1 (Baf) for 45 min. before imaging. (A) pH images before and after treatment with Bafilomycin A1. The ratio of green to red in every pixel is converted to pH *via* the calibration curve and color coded on a linear scale according to pH. The N indicates the location of the nucleus. Scale bar, 10 μm. (B) Histogram showing pH distributions by pixel intensity quantification in approximately 1000 individual endosomes/lysosomes based on the type of images presented in (A). Mean ± SEM (standard error of the mean)(n = 9 images).

After the treatment the color has clearly changed from yellow/orange to blue/green indicating an increase in pH. As bafilomycin A_1 inhibits the proton pump that acidifies lysosomes and thus increases the pH of the lysosomes, which is also supportive of lysosomal localization. The pH histograms presented in Fig. 6b gives a mean pH of 4.3 before treatment and 6.3 after the treatment confirming what is observed in the images. From these pH distributions, it is clear that the sensor is well suited to measure pH in the endosome-lysosome pathway as only 2% of measurements of the ratios obtained from the images of the bafilomycin treated sample falls outside the sensor's range.

Conclusions

We have demonstrated the first synthesis, characterization and utilization of a shell cross-linked core–shell–corona micelle based ratiometric pH nanosensor (SCMN) for intracellular measurements. ATRP and the principle of self-assembly were used to prepare polymeric micelles having a well-defined core–shell–corona morphology. The reinforcement of the weak hydrophobic interactions between the unimers of the micelle was provided by covalent cross-linking using an amidation reaction. The stabilized micelles were converted to ratiometric pH nanosensors by fluorophore conjugation at the shell region. An *In vitro* pH calibration curve for the nanosensor was constructed by fluorescence measurements, which showed a broad pH sensitivity range of the triple-labelled nanosensors. Fluorescence measurements also confirmed the fast response and reversibility of these pH nanosensors. Cell uptake experiments of the nanosensors were performed and pH distributions of HeLa cells were monitored. This showed that the sensor was able to pass the cell membrane by cellular internalization and respond to pH changes within the endosome-lysosome cellular environment. This design of triple fluorophore labelled sensors enable ratiometric pH measurements within the whole endocytic pathway in cells.

Acknowledgements

The authors would like to thank Kræftens Bekæmpelse and the Danish Research Council for Technology and Production for financial support.

References

1 D. Lagadic-Gossmann, L. Huc and V. Lecureur, *Cell Death Differ.*, 2004, **11**, 953–961.
2 S. T. Whitten, E. B. García-Moreno and V. J. Hilser, *Proc. Natl. Acad. Sci. U. S. A.*, 2005, **102**, 4282–4287.
3 J. R. Casey, S. Grinstein and J. Orlowski, *Nat. Rev. Mol. Cell Biol.*, 2010, **11**, 50–61.
4 A. Asokan and M. J. Cho, *J. Pharm. Sci.*, 2002, **91**, 903–913.
5 T. L. Andresen, S. S. Jensen and K. Jørgensen, *Prog. Lipid Res.*, 2005, **44**, 68–97.
6 H. A. Clark, R. Kopelman, R. Tjalkens and M. A. Philbert, *Anal. Chem.*, 1999, **71**, 4837–4843.
7 J. Ji, N. Rosenzweig, C. Griffin and Z. Rosenzweig, *Anal. Chem.*, 2000, **72**, 3497–3503.
8 H. Sun, T. L. Andresen, R. V. Benjaminsen and K. Almdal, *J. Biomed. Nanotechnol.*, 2009, **5**, 676–682.
9 H. Sun, K. Almdal and T. L. Andresen, *Chem. Commun.*, 2011, **47**, 5268–5270.
10 J. Peng, X. He, K. Wang, W. Tan, Y. Wang and Y. Liu, *Anal. Bioanal. Chem.*, 2007, **388**, 645–654.
11 R. V. Benjaminsen, H. Sun, J. R. Henriksen, N. M. Christensen, K. Almdal and T. L. Andresen, *ACS Nano*, 2011, **5**, 5864–5873.
12 V. M. Chauhan, G. Orsi, A. Brown, D. I. Pritchard and J. W. Aylott, *ACS Nano*, 2013, **7**, 5577–5587.
13 S. M. Moghimi, A. C. Hunter and J. C. Murray, *Pharm. Rev.*, 2001, **53**, 283–318.
14 V. P. Torchilin, *J. Controlled Release*, 2001, **73**, 137–172.
15 E. K. Pramod Kumar, K. Almdal and T. L. Andresen, *Chem. Commun.*, 2012, **48**, 4776–4778.
16 E. K. P. Kumar, L. N. Feldborg, K. Almdal and T. L. Andresen, *Chem. Mater.*, 2013, **25**, 1496–1501.

17 K. Matyjaszewski and N. V. Tsarevsky, *Nat. Chem.*, 2009, **1**, 276–288.
18 L. Zhang and A. Eisenberg, *Science*, 1995, **268**, 1728–1731.
19 L. Zhang, K. Yu and A. Eisenberg, *Science*, 1996, **272**, 1777–1779.
20 H. Sun, R. V. Benjaminsen, K. Almdal and T. L. Andresen, *Bioconjugate Chem.*, 2012, **23**, 2247–2255.
21 R. K. O'Reilly, C. J. Hawker and K. L. Wooley, *Chem. Soc. Rev.*, 2006, **35**, 1068–1083.
22 E. S. Read and S. P. Armes, *Chem. Commun.*, 2007, 3021–3035.
23 S. Liu, J. V. M. Weaver, Y. Tang, N. C. Billingham, S. P. Armes and K. Tribe, *Macromolecules*, 2002, **35**, 6121–6131.
24 M.-H. l. n. Dufresne and J.-C. Leroux, *Pharm. Res.*, 2004, **21**, 160–169.
25 E. Kaiser, R. L. Colescott, C. D. Bossinger and P. I. Cook, *Anal. Biochem.*, 1970, **34**, 595–598.